Available online at www.sciencedirect.com
ScienceDirect
Trans. Nonferrous Met. Soc. China 30(2020) 2079−2089
Transactions of Nonferrous Metals Society of China
www.tnmsc.cn

Effect of Sn content on microstructure and tensile properties of as-cast and as-extruded Mg−8Li−3Al−(1,2,3)Sn alloys

Xiao-yang CHEN, Yang ZHANG, Meng-qi CONG, Ya-lin LU, Xiao-ping LI

Key Laboratory of Advanced Materials Design and Additive Manufacturing of Jiangsu Province, Jiangsu University of Technology, Changzhou 213001, China

Received 28 November 2019; accepted 16 July 2020

Abstract: The effects of Sn content on microstructure and tensile properties of as-cast and as-extruded Mg−8Li−3Al−(1,2,3)Sn (wt.%) alloys were investigated by X-ray diffractometry (XRD), optical microscopy (OM), scanning electron microscopy (SEM) and tensile test. It is found that, as-cast Mg−8Li−3Al−(1,2,3)Sn alloys consist of α-Mg+β-Li duplex matrix, $MgLiAl_2$ and Li_2MgSn phases. Increasing Sn content leads to grain refinement of α-Mg dendrites and increase in content of Li_2MgSn phase. During hot extrusion, complete dynamic recrystallization (DRX) takes place in β-Li phase while incomplete DRX takes place in α-Mg phase. As Sn content is increased, the volume fraction of DRXed α-Mg grains is increased and the average grain size of DRXed α-Mg grains is decreased. Increasing Sn content is beneficial to strength but harmful to ductility for as-cast Mg−8Li−3Al−(1,2,3)Sn alloys. Tensile properties of Mg−8Li−3Al−(1,2,3)Sn alloys are improved significantly via hot extrusion and Mg−8Li−3Al−2Sn alloy exhibits the best tensile properties.

Key words: Mg−Li−Al−Sn alloy; as-cast state; recrystallization; microstructure; tensile properties

1 Introduction

Since Li (ρ_{Li}=0.534 g/cm^3) has the lowest density among metallic elements, the addition of Li can further reduce the density of Mg alloys [1−3]. The addition of Li can also improve the plastic deformation capacity of Mg alloys, which is important since the plastic deformation capacity of conventional Mg alloys is restricted by the hexagonal close-packed (HCP) structure [4−6]. However, poor mechanical properties of binary Mg−Li alloys cannot meet the requirement for application as structural materials [7−10]. Therefore, the design of new Mg−Li alloys is mainly aimed at improving the mechanical properties of Mg−Li alloys, especially the strength.

The addition of different elements is usually employed to improve the mechanical properties of Mg−Li alloys. Due to its good strengthening effect, Al has been the most frequently used element so far. Existing commercial Mg−Li alloys are mainly developed based on Mg−Li−Al alloys [11,12]. However, as age softening phenomenon often occurs in Mg−Li−Al alloys, the mechanical properties are still unsatisfied [13,14]. The alloy design of Mg−Li−Al alloy series is aimed at further improving the strength and thermal stability. The co-addition of Al and other elements in Mg−Li alloys can lead to the formation of different intermetallic phases and contribute to alloy strengthening simultaneously, which has been proven to be an effective design strategy for Mg−Li alloys. YANG et al [15] found that the addition of

Foundation item: Project (51601076) supported by the National Natural Science Foundation of China; Project (17KJA430005) supported by the Natural Science Fund for Colleges and Universities in Jiangsu Province, China; Project (2019M650096) supported by China Postdoctoral Science Foundation

Corresponding author: Yang ZHANG; Tel: +86-519-86953210; E-mail: zhangyang@jsut.edu.cn

DOI: 10.1016/S1003-6326(20)65362-6

Sr led to the formation of thermal-stable Al_4Sr phase in Mg−9Li−3Al−*x*Sr alloys, and the best tensile strength was achieved when Sr content was 2.5 wt.%.

JIANG et al [16] reported that Sn element induced the formation of Sn-containing inter-metallic phases in Mg−9Li alloy. SON et al [17,18] found that the co-added Sn and Mn elements improved the strength of Mg−Li−Al(Zn) alloys. Recently, FU et al [19] reported that the co-addition of Al and Sn in Mg−8Li−1Al−0.5Sn alloy exhibited good strengthening effect. However, the study on Mg−Li−Al−Sn alloys is still limited up to now. Few relevant literatures about the effect of Sn content on microstructure and tensile properties of Mg−Li−Al−Sn alloys can be referred. The variation of Sn content would influence the phase composition, microstructure and corresponding mechanical properties of Mg−Li−Al−Sn alloys. Therefore, it is necessary to study the effect of Sn content on microstructure and tensile properties of Mg−Li−Al−Sn alloys and obtain the potential optimized alloy composition.

In this study, a series of Mg−8Li−3Al−(1,2,3)Sn (wt.%) alloys were prepared by vacuum induction melting and then subjected to hot extrusion. The microstructure and tensile properties of Mg−8Li−3Al−(1,2,3)Sn alloys in as-cast and as-extruded states were investigated systematically. The influencing mechanism of Sn content on microstructure evolution and tensile properties was also discussed.

2 Experimental

Commercially pure Mg, Li, Al and Sn were used to prepare Mg−8Li−3Al−(1,2,3)Sn (LAT831, LAT832 and LAT833) alloys. The melting and casting of as-cast ingots were done in a vacuum induction furnace with the protective atmosphere of Ar gas. Cylindrical extrusion billets were cut from the casting ingots and then machined into *d*40 mm × 60 mm. Before hot extrusion, the extrusion billets were heated to 200 °C and held for 60 min. Hot extrusion was done at 200 °C and the extrusion ratio was kept to be 9:1.

Phase composition of as-cast alloys was characterized by X-ray diffraction (XRD, Panalytical XPERT POWDER). Microstructure of as-cast and as-extruded alloys was characterized by optical microscope (OM, Zeiss Primotech) and scanning electron microscope (SEM, Zeiss Simga 500, equipped with energy dispersive spectrometer (EDS) and electron back-scattered diffraction (EBSD)). Quantitative metallurgical analysis was carried out by quantitative image analysis software (image pro plus 5.0). Ambient temperature tensile test was done with a universal testing machine (WANCE CMT−5205) according to ISO 6892-1: 2009. Tensile specimens of as-cast samples were cut from the as-cast ingots and tensile specimens of as-extruded samples were cut from the as-extruded bars along the extrusion direction. The gauge dimension was 10 mm × 3 mm × 2 mm and the strain rate was 1.67×10^{-3} s^{-1}. For each sample, at least three specimens were tested and the average was taken. Fracture morphology of tensile tested samples was also observed by SEM.

3 Results and discussion

3.1 Microstructure of as-cast Mg−8Li−3Al−(1,2,3)Sn alloys

Figure 1 presents the XRD patterns of as-cast Mg−8Li−3Al−(1,2,3)Sn alloys. The diffraction peaks of both *α*-Mg phase and *β*-Li phase are detected in as-cast Mg−8Li−3Al−(1,2,3)Sn alloys, which is consistent with Mg−Li binary phase diagram. The diffraction peaks of $MgLiAl_2$ phase are also detected and the rest diffraction peaks correspond to Mg_2Sn phase or Li_2MgSn phase. Since the lattice parameters of Mg_2Sn phase and Li_2MgSn phase are too close, it is difficult to distinguish these two phases through XRD analysis. It is obvious that, with the increase of Sn content,

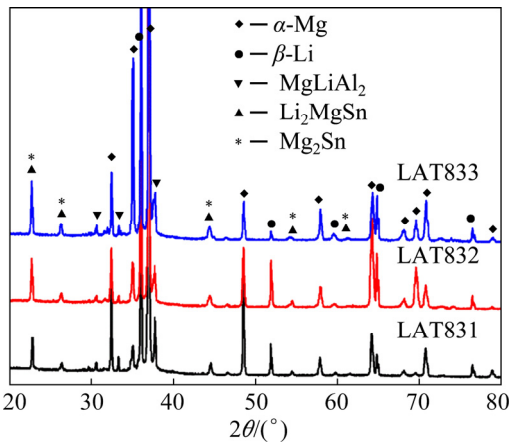

Fig. 1 XRD patterns of as-cast Mg−8Li−3Al−(1,2,3)Sn alloys

the intensity of diffraction peaks corresponding to Mg_2Sn phase or Li_2MgSn phase is enhanced gradually.

Figure 2 shows the microstructures of as-cast Mg−8Li−3Al−(1,2,3)Sn alloys observed by OM. As-cast Mg−8Li−3Al−(1,2,3)Sn alloys exhibit typical α-Mg+β-Li duplex structure. The white coarse dendrites are α-Mg phases and the surrounding grey grains are β-Li phases. It is observed that, with the increase of Sn content, α-Mg dendrites in as-cast Mg−8Li−3Al−(1,2,3)Sn alloys are significantly refined. According to the quantitative analysis result, the average grain size of α-Mg grains is ~252 μm in as-cast LAT831 alloy, and it decreases to ~191 μm in as-cast LAT832 alloy and ~133 μm in as-cast LAT833 alloy. The

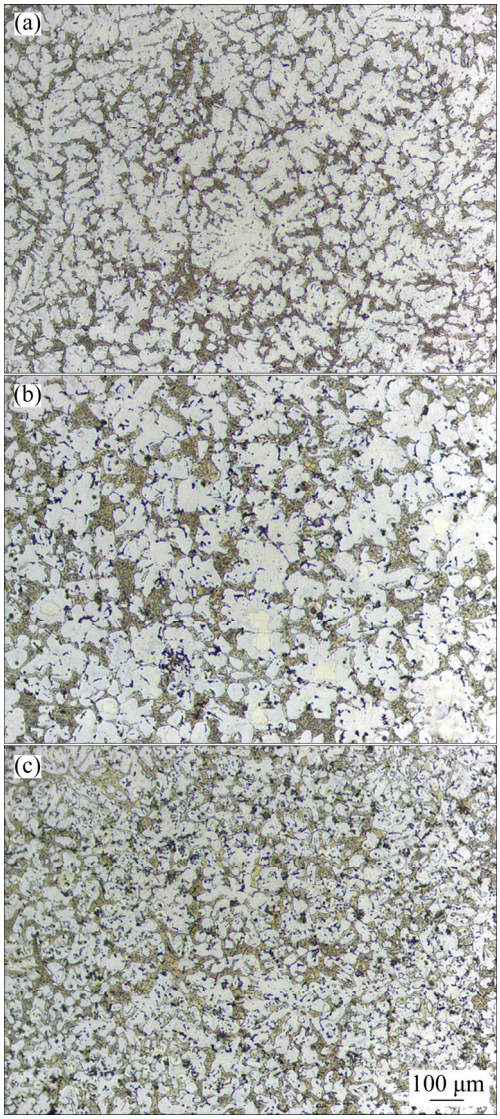

Fig. 2 Microstructures of as-cast Mg−8Li−3Al−(1,2,3)Sn alloys observed by OM: (a) LAT831; (b) LAT832; (c) LAT833

grain refinement in as-cast alloys is usually achieved by promoting the nucleation and/or restricting the growth of nuclei [20]. In as-cast Mg−8Li−3Al−(1,2,3)Sn alloys, the intermetallic phases form after the nucleation of α-Mg grains and cannot act as nucleation sites. Therefore, growth restriction effect of Sn element is the main reason for grain refinement of α-Mg grains. The capability of growth restriction effect of Sn element during the growth of α-Mg nuclei is closely related to Sn content. The high concentration of Sn element restricts the dendritic growth of α-Mg grains during solidification and results in the grain refinement.

Figures 3(a−c) present the microstructures of as-cast Mg−8Li−3Al−(1,2,3)Sn alloys observed by backscattered electron (BSE)-SEM. It is obvious that, there are two kinds of intermetallic phases in as-cast Mg−8Li−3Al−(1,2,3)Sn alloys. One is the small particle-like intermetallic phase which distributes only in β-Li phase and the other is the well-developed feather-like intermetallic phase which distributes randomly in the matrix. The small intermetallic phase is grey while the feather-like phase is bright in color, which indicates that the main elements of these two intermetallic phases are different. Figure 3(d) shows a high magnification image of as-cast LAT833 sample and Figs. 3(e, f) show the corresponding EDS results of Points A and B in Fig. 3(d). EDS results show that the small grey phase is rich in Mg and Al while the coarse bright phase is rich in Mg and Sn. Since Li element is undetectable in EDS, no Li element is detected in Point A or B. Considering the above XRD pattern, the small grey intermetallic phases are determined to be $MgLiAl_2$ phase and the coarse bright intermetallic phases are Sn-containing phases. According to Mg−Li−Sn phase diagram, Li_2MgSn phase is chemically steady in Mg−8Li−(1,2,3)Sn alloys. JIANG et al [21] reported that, Mg_2Sn and Li_2MgSn phases coexisted in Mg−5Sn−0.3Li alloy, while only Li_2MgSn phase was found in Mg−5Sn−1Li alloy. These results proved that, when the atomic ratio of Li to Sn reached 3:1, Li_2MgSn phase would be the only intermetallic phase in Mg−Sn−Li alloys. In this study, although the formation of $MgLiAl_2$ phase consumes a part of Li element, the atomic ratio of Li to Sn in as-cast Mg−8Li−3Al−(1,2,3)Sn alloys exceeds 3:1 substantially. Moreover, the morphology of Sn-containing phase in as-cast Mg−8Li−3Al−(1,2,3)Sn

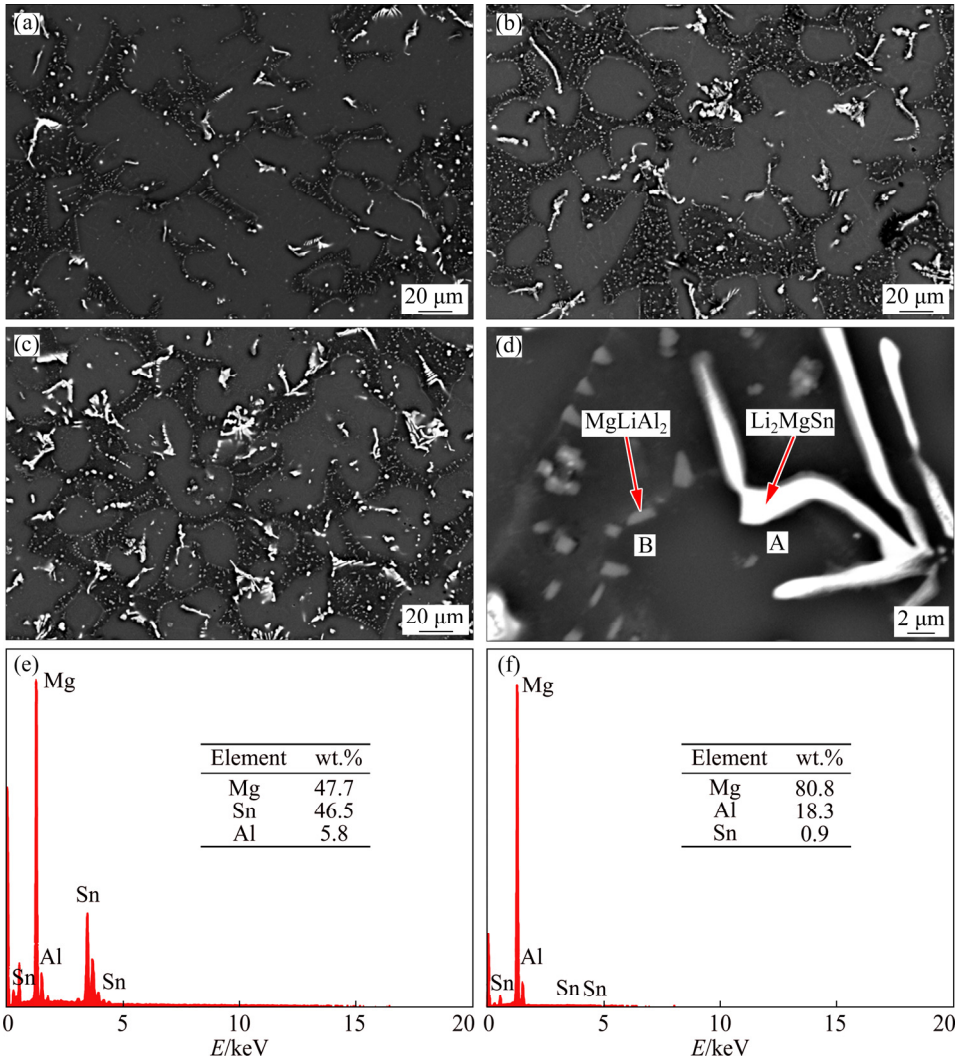

Fig. 3 BSE-SEM images (a−d) and EDS results (e, f) of as-cast Mg−8Li−3Al−(1,2,3)Sn alloys: (a) LAT831; (b) LAT832; (c, d) LAT833; (e) Point A; (f) Point B

alloys is similar to that in previous report about the morphology of Li_2MgSn phase [22]. Therefore, it is reasonable to conclude that, the coarse bright phases in Mg−8Li−3Al−(1,2,3)Sn alloys are Li_2MgSn phases. The volume fraction of Li_2MgSn phase increases from 2.2% in as-cast LAT831 alloy to 3.4% in as-cast LAT832 alloy and 5.0% in as-cast LAT833 alloy. Moreover, Li_2MgSn phase in as-cast Mg−8Li−3Al−(1,2,3)Sn alloys coarsens significantly with the increase of Sn content. However, the change of Sn content has little influence on the content or morphology of $MgLiAl_2$ phase.

3.2 Microstructure of as-extruded Mg−8Li−3Al−(1,2,3)Sn alloys

Figure 4 shows microstructures of as-extruded Mg−8Li−3Al−(1,2,3)Sn alloys observed by OM. The α-Mg+β-Li duplex structure is elongated during hot extrusion and banded structure forms in as-extruded Mg−8Li−3Al−(1,2,3)Sn alloys. The coarse α-Mg dendrites are stripped while β-Li phase distributes among the elongated α-Mg grains.

Figure 5 presents the microstructures of as-extruded Mg−8Li−3Al−(1,2,3)Sn alloys observed by secondary electron (SE)-SEM. The SEM images of as-extruded Mg−8Li−3Al−(1,2,3)Sn alloys confirm that complete dynamic recrystallization (DRX) takes place in β-Li phase and DRXed β-Li grains turn to be fine and equiaxed. It is difficult to judge whether DRX takes place in α-Mg phase through SEM images and it is conducted by the following EBSD characterization. Moreover, the well-developed feather-like Li_2MgSn phase is

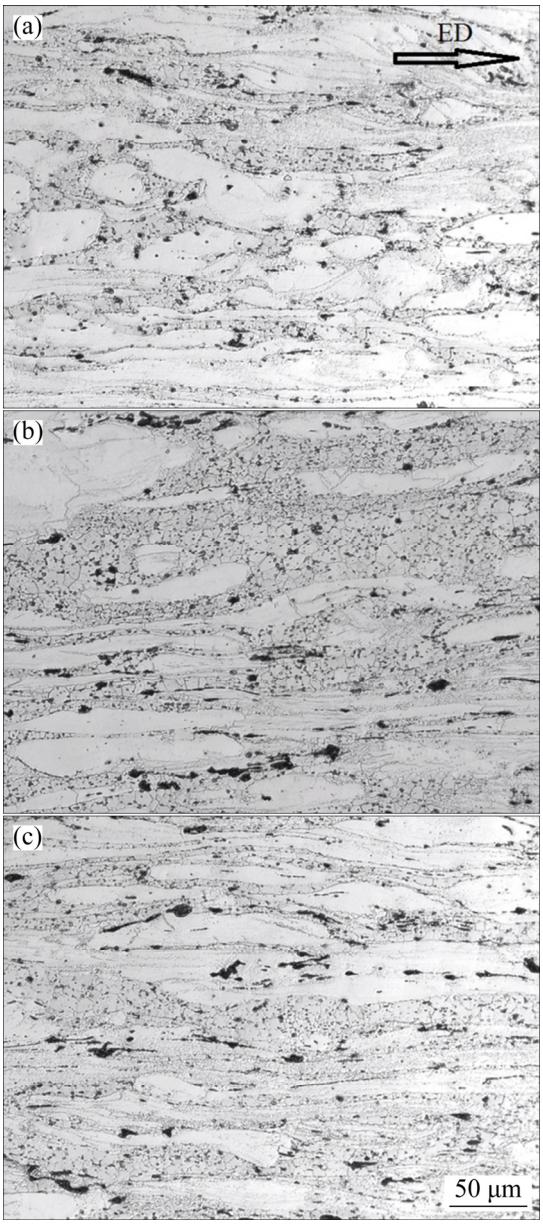

Fig. 4 Microstructures of as-extruded Mg−8Li−3Al−(1,2,3)Sn alloys observed by OM (ED — Extrusion direction): (a) LAT831; (b) LAT832; (c) LAT833

crushed into particles and redistributes along the extrusion direction. It is found that, the crushing of Li_2MgSn phase during hot extrusion is uneven. The average sizes of broken Li_2MgSn particles in as-extruded LAT831, LAT832 and LAT833 alloys are 3.3, 3.5 and 5.9 μm, respectively. With the coarsening of Li_2MgSn phase in as-cast Mg−8Li−3Al−(1,2,3)Sn alloys, the refining effect of hot extrusion on Li_2MgSn phase is weakened. The small $MgLiAl_2$ particles still distribute in β-Li phase and show little change after hot extrusion.

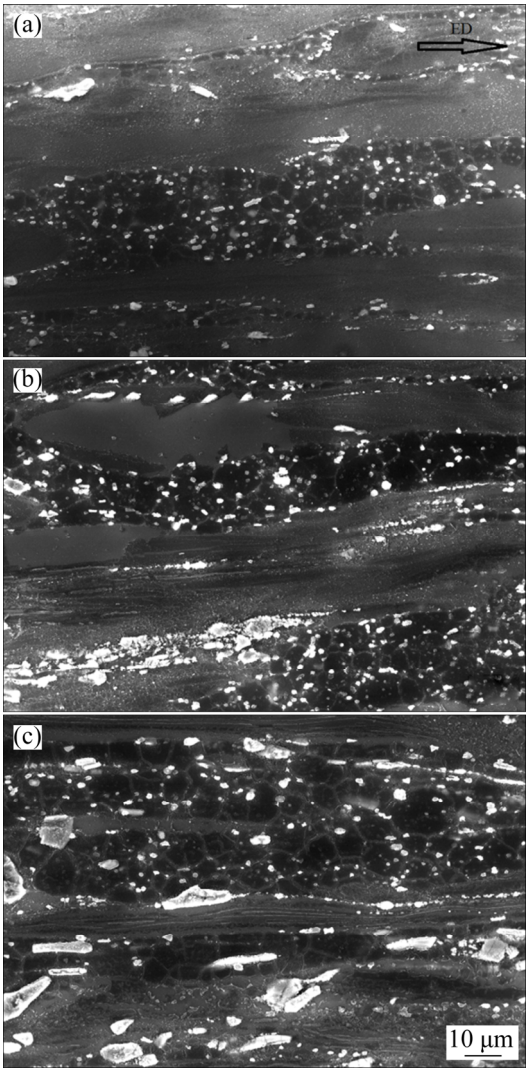

Fig. 5 Microstructures of as-extruded Mg−8Li−3Al−(1,2,3)Sn alloys observed by SE-SEM (ED—Extrusion direction): (a) LAT831; (b) LAT832; (c) LAT833

3.3 EBSD results of as-extruded Mg−8Li−3Al−(1, 2, 3)Sn alloys

Figure 6 presents the inverse pole figures of α-Mg phase in as-extruded Mg−8Li−3Al−(1,2,3)Sn alloys obtained by EBSD. It is clearly observed from the inverse pole figures that, hot extrusion induces incomplete DRX in α-Mg phase. Compared to as-cast Mg−8Li−3Al−(1,2,3)Sn alloys, DRXed α-Mg grains are significantly refined. Meanwhile, the coarse un-DRXed α-Mg grains are elongated. According to the quantitative analysis results obtained by EBSD, as Sn content increases from 1 to 3 wt.%, the volume fraction of DRXed α-Mg grains increases from 42.4% in as-extruded LAT831 alloy to 48.6% in as-extruded LAT832 alloy and 56.8% in as-extruded LAT833 alloy. Meanwhile,

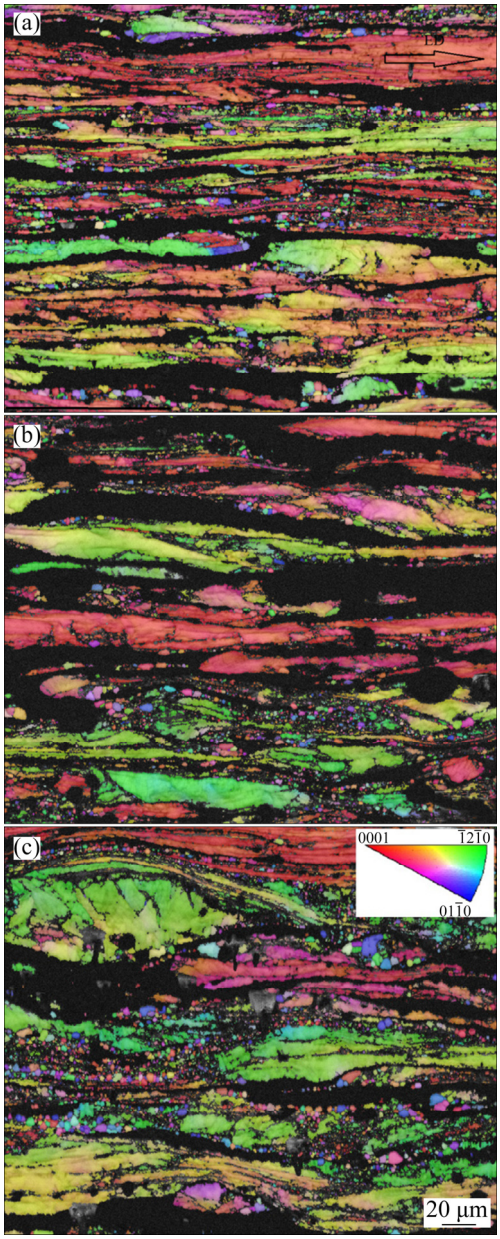

Fig. 6 Inverse pole figures of α-Mg phase in as-extruded Mg−8Li−3Al−(1,2,3)Sn alloys obtained by EBSD: (a) LAT831; (b) LAT832; (c) LAT833

the average grain size of DRXed α-Mg grains decreases from 5.1 μm in as-extruded LAT831 alloy to 3.3 μm in as-extruded LAT832 alloy and 2.9 μm in as-extruded LAT833 alloy. Different from single-phase alloys, only the slip system of one phase is required to be activated during the coordinated deformation of duplex structure. Since soft β-Li phase is easy to be deformed, it is deformed first. As the applied force is increased, the hard α-Mg phase slips and enables the plastically-compatible deformation [23,24]. As β-Li phase can allow much more uniform deformation than α-Mg phase, the driving force accumulated for DRX of α-Mg phase is reduced. Therefore, DRX process of α-Mg phase during hot extrusion is inhibited. Moreover, particle stimulated nucleation (PSN) mechanism plays an important role in DRX of Mg−8Li−3Al−(1,2,3)Sn alloys [25]. Intermetallic phases could promote the dislocation accumulation, increase the driving force and play the role of nucleation sites for DRX. In this study, $MgLiAl_2$ phase and Li_2MgSn phase coexist in as-cast Mg−8Li−3Al−(1,2,3)Sn alloys. $MgLiAl_2$ phase distributes densely in β-Li phase and provides sufficient nucleation sites for DRX of β-Li phase. Moreover, dense $MgLiAl_2$ phase can also inhibit the growth of DRXed β-Li grains via hindering grain boundary migration [26]. As for α-Mg phase, it is obvious that increasing the volume fraction of Li_2MgSn phase provides more nucleation sites and therefore leads to increased volume fraction of α-Mg grains and reduced grain size of DRXed α-Mg grains.

Figure 7 presents the pole figures of α-Mg phase in as-extruded Mg−8Li−3Al−(1,2,3)Sn alloys obtained by EBSD. Typical ED//(0001) extrusion texture forms in α-Mg phase in as-extruded Mg−8Li−3Al−(1,2,3)Sn alloys. Due to the existence of coarse un-DRXed α-Mg grains, the texture intensity is relatively high and the peak intensity varies from 16.9 to 19.2.

3.4 Tensile properties of as-cast and as-extruded Mg−8Li−3Al−(1,2,3)Sn alloys

Figure 8 shows tensile properties of Mg−8Li−3Al−(1,2,3)Sn alloys and the data are presented in Table 1. As Sn content is increased from 1 to 3 wt.%, the strength of as-cast alloys is increased while the ductility is decreased continuously. YS and UTS are increased by 34% and 8% while elongation is decreased by 38%. LAT833 alloy exhibits the highest strength among as-cast Mg−8Li−3Al−(1,2,3)Sn alloys, and YS, UTS and elongation of as-cast LAT833 alloy are 156 MPa, 190 MPa and 9.9%, respectively. However, with the increase of Sn content, strength and ductility of as-extruded Mg−8Li−3Al−(1,2,3)Sn alloys are increased first and then decreased. LAT832 alloy possesses the best tensile properties among as-extruded alloys and YS, UTS and elongation of as-extruded LAT832 alloy are 270 MPa, 297 MPa and 20.8%, respectively. It is confirmed that the hot

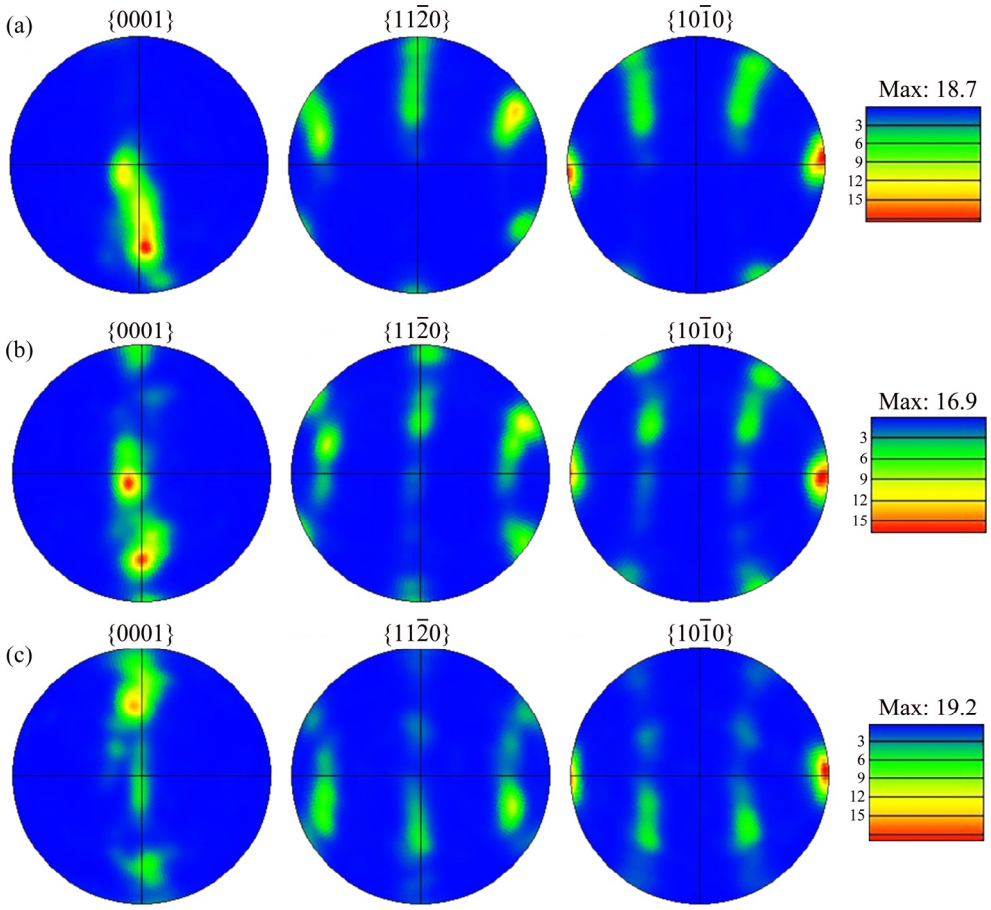

Fig. 7 Pole figures of α-Mg phase in as-extruded Mg−8Li−3Al−(1,2,3)Sn alloys obtained by EBSD: (a) LAT831; (b) LAT832; (c) LAT833

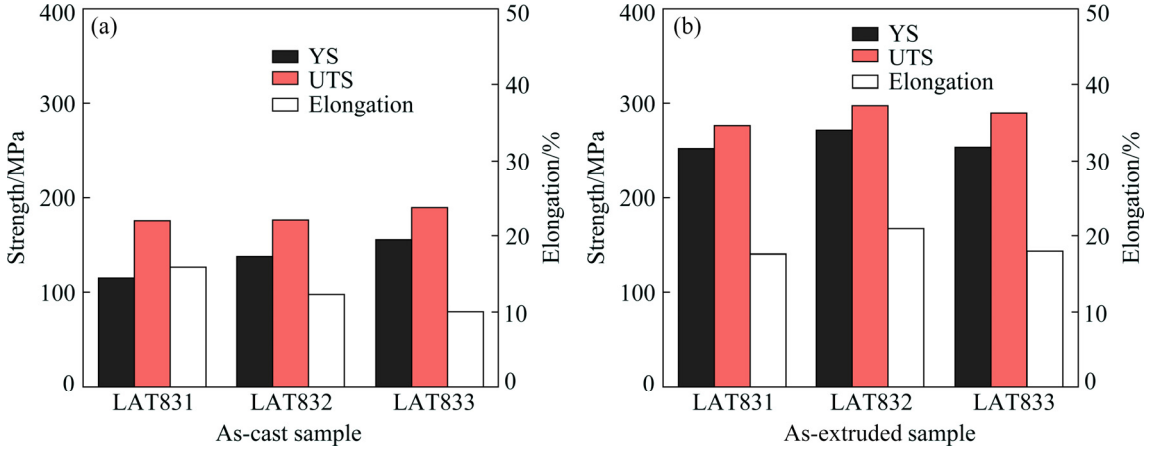

Fig. 8 Tensile properties of Mg−8Li−3Al−(1,2,3)Sn alloys: (a) As-cast; (b) As-extruded

extrusion is beneficial to improving tensile properties of Mg−8Li−3Al−(1,2,3)Sn alloys. Compared to as-cast alloys, YS and UTS are improved by 63%−116% and 52%−67%, respectively, and elongation of as-extruded alloys is improved by 9%−81%.

As for as-cast Mg−8Li−3Al−(1,2,3)Sn alloys, increase of Sn content leads to continuous increase in strength but decrease in ductility. The continuous increase in strength of as-cast Mg−8Li−3Al−(1,2,3)Sn alloys is mainly attributed to the grain refinement of α-Mg phase. As shown in Fig. 2, the average size of α-Mg grains decreases from 252 to 133 μm when Sn content increases from 1 to

Table 1 YS, UTS and elongation of Mg−8Li−3Al−(1,2,3)Sn alloys

Alloy	State	Yield strength/ MPa	Ultimate tensile strength/ MPa	Elongation to failure/ %
LAT831	As-cast	116±3	176±7	15.9±1.2
	As-extruded	251±2	275±4	17.4±1.4
LAT832	As-cast	138±2	177±5	12.3±0.8
	As-extruded	270±4	297±5	20.8±1.5
LAT833	As-cast	156±3	190±3	9.9±2.3
	As-extruded	253±6	289±8	17.9±2.1

3 wt.%. During deformation of duplex Mg−Li alloys, α-Mg phase bears most of the stress. The grain refinement of α-Mg grains in as-cast Mg−8Li−3Al−(1,2,3)Sn alloys increases the grain boundary area and the difficulty of dislocation movement is enhanced. Al element dissolving in α-Mg+β-Li matrix can also contribute to solid solution strengthening. Since most of Sn element exists in Li_2MgSn phase, the solid solution strengthening effect of Sn element is limited. $MgLiAl_2$ phase only distributes in β-Li phase and its strengthening effect is poor since β-Li phase is soft. As Li_2MgSn phase in as-cast Mg−8Li−3Al−(1,2,3)Sn alloys is coarse and brittle, its strengthening effect is also negligible. Moreover, due to the increased volume fraction of brittle feather-like Li_2MgSn phase, the ductility of as-cast Mg−8Li−3Al−(1,2,3)Sn alloys is deteriorated significantly with the increase of Sn content.

Tensile test results in Fig. 8 and Table 1 confirm that, hot extrusion is beneficial to comprehensive tensile properties of Mg−8Li−3Al−(1,2,3)Sn alloys. In as-extruded Mg−8Li−3Al−(1,2,3)Sn alloys, YS, UTS and elongation all reach the peak values when Sn content is 2 wt.%. In other words, LAT832 alloy exhibits the best comprehensive tensile properties among as-extruded Mg−8Li−3Al−(1,2,3)Sn alloys. Further increasing Sn content to 3 wt.% leads to decrease in strength and ductility simultaneously. The enhancement in comprehensive tensile properties is explained based on the following reasons [27−30]: (1) Due to the DRX effect, the grain size in as-extruded Mg−8Li−3Al−(1,2,3)Sn alloys is reduced, which contributes to further grain refinement strengthening; (2) As shown in Fig. 7, strong basal texture is formed in as-extruded alloys and it gives rise to texture strengthening; (3) Coarse feather-like Li_2MgSn phase is crushed into particles and the strengthening effect of crushed Li_2MgSn particles in as-extruded Mg−8Li−3Al−(1,2,3)Sn alloys is stronger than that of the coarse Li_2MgSn phase in as-cast Mg−8Li−3Al−(1,2,3)Sn alloys. Moreover, due to the crush of Li_2MgSn phase during hot extrusion, negative influence of coarse Li_2MgSn phase on ductility of as-cast alloys is weakened and the ductility of as-extruded Mg−8Li−3Al−(1,2,3)Sn alloys is improved. It is found that, the range of improvement in ductility after hot extrusion of LAT832 and LAT833 alloys is much higher than that of LAT831 alloy. Considering the corresponding increase in content of Li_2MgSn phase in LAT832 and LAT833 alloys, it is reasonable to conclude that the crush of coarse Li_2MgSn phase is the main reason for enhancement in ductility of as-extruded Mg−8Li−3Al−(1,2,3)Sn alloys after hot extrusion. As shown in Fig. 6, the volume fraction of DRXed α-Mg grains in as-extruded LAT833 alloy is higher than that in as-extruded LAT831 and LAT832 alloys, and the average grain size of DRXed α-Mg grains in as-extruded LAT833 alloy is larger than that in as-extruded LAT831 and LAT832 alloys. As shown Fig. 7, the texture intensity of as-extruded Mg−8Li−3Al−(1,2,3)Sn alloys is close to each other. Therefore, the insufficient crush of Li_2MgSn phase in as-extruded LAT833 alloy is the possible reason for the worsening of strength and ductility. As shown in Fig. 5(c), the size of broken Li_2MgSn particles in as-extruded LAT833 alloy is still large and such large intermetallic particles are harmful to both strength and ductility.

3.5 Fracture morphology of as-cast and as-extruded Mg−8Li−3Al−(1,2,3)Sn alloys

Figure 9 shows the fracture morphology of tensile tested Mg−8Li−3Al−(1,2,3)Sn samples. The cleavage planes and dimples coexist on the fracture surfaces of as-cast Mg−8Li−3Al−(1,2,3)Sn alloys, which indicates that the fracture mode of as-cast alloys is ductile and brittle mixed. Moreover, more intermetallic particles are found on the fracture surfaces with increase of Sn content, which is likely to serve as crack initiation sites under external force and leads to the reduction of ductility. Compared with as-cast alloys, more dimples are found in

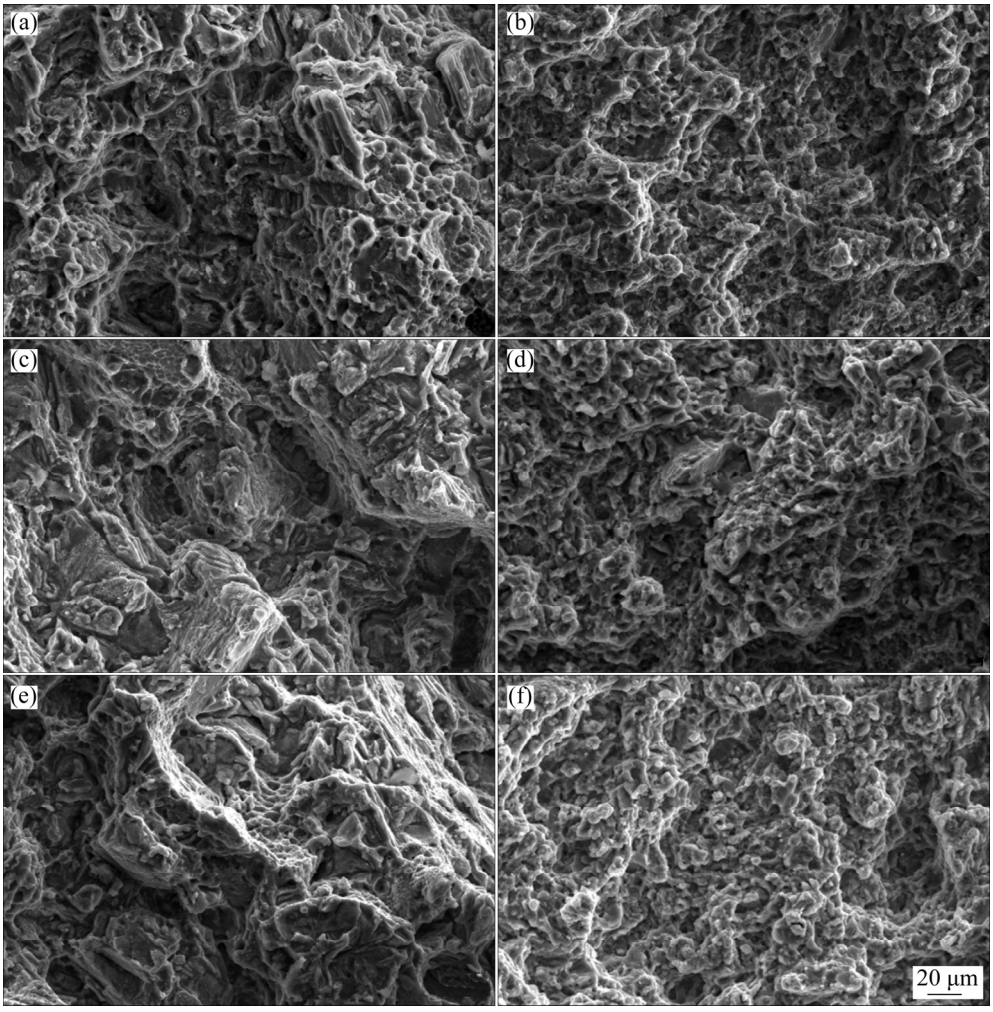

Fig. 9 Fracture morphologies of tensile tested Mg−8Li−3Al−(1,2,3)Sn samples: (a) As-cast LAT831; (b) As-extruded LAT831; (c) As-cast LAT832; (d) As-extruded LAT832; (e) As-cast LAT833; (f) As-extruded LAT833

as-extruded Mg−8Li−3Al−(1,2,3)Sn alloys and the cleavage planes are seldom found. Some crushed intermetallic particles are found on fracture surfaces of as-extruded LAT832 and LAT833 alloys.

4 Conclusions

(1) As-cast Mg−8Li−3Al−(1,2,3)Sn alloys consist of α-Mg+β-Li duplex matrix, $MgLiAl_2$ phase and Li_2MgSn phase. As Sn content is increased, α-Mg dendrites are refined and the content of Li_2MgSn phase is increased significantly.

(2) The α-Mg+β-Li duplex structure is elongated and grains are refined during hot extrusion. DRX in β-Li phase is complete and DRX in α-Mg phase is incomplete. As Sn content is increased, the volume fraction of DRXed α-Mg grains is increased and the average grain size of DRXed α-Mg grains is decreased.

(3) The increase of Sn content leads to continuous increase in strength but decrease in ductility for as-cast Mg−8Li−3Al−(1,2,3)Sn alloys. Hot extrusion improves the tensile properties of Mg−8Li−3Al−(1,2,3)Sn alloys and Mg−8Li−3Al−2Sn alloy exhibits the best tensile properties. The improvement in tensile properties after hot extrusion is attributed to further grain refinement, strong basal texture and crush of Li_2MgSn phase.

References

[1] SUN Yue-hua, WANG Ri-chu, PENG Chao-qun, FENG Yan, YANG Ming. Recent progress in Mg−Li matrix composites [J]. Transactions of Nonferrous Metals Society of China, 2019, 29(1): 1−14.

[2] SUN Yue-hua, WANG Ri-chu, PENG Chao-qun, FENG Yan,

YANG Ming. Corrosion behavior and surface treatment of superlight Mg−Li alloys [J]. Transactions of Nonferrous Metals Society of China, 2017, 27(7): 1455−1475.

[3] LIU Gang, MA Zhen-duo, WEI Guo-bing, XU Tian-cai, ZHANG Xi, YANG Yan, XIE Wei-dong, PENG Xiao-dong. Microstructure, tensile properties and corrosion behavior of friction stir processed Mg−9Li−1Zn alloy [J]. Journal of Materials Processing Technology, 2019, 267: 393−402.

[4] DING Hong-bo, LIU Qiang, ZHOU Hai-tao, ZHOU Xiao, ATRENS A. Effect of thermal-mechanical processing on microstructure and mechanical properties of duplex-phase Mg−8Li−3Al−0.4Y alloy [J]. Transactions of Nonferrous Metals Society of China, 2017, 27(12): 2587−2597.

[5] ZHOU Yu-cheng, CHEN Zhao-yun, JI Jing-han, SUN Zhi-jie. Effects of second phases on deformation behavior and dynamic recrystallization of as-cast Mg−4.3Li−4.1Zn−1.4Y alloy during hot compression [J]. Journal of Alloys and Compounds, 2019, 770: 540−548.

[6] JI Hao, LIU Wen-cai, WU Guo-hua, OUYANG Si-jie, GAO Zhan-kui, PENG Xiang, DING Wen-jiang. Influence of Er addition on microstructure and mechanical properties of as-cast Mg−10Li−5Zn alloy [J]. Materials Science and Engineering A, 2019, 739: 395−403.

[7] WU R, YAN Y, WANG G, MURR L E, HAN W, ZHANG Z, ZHANG M. Recent progress in magnesium-lithium alloys [J]. International Materials Reviews, 2015, 60(2): 65−100.

[8] ZHAO Jiong, LI Zhong-quan, LIU Wen-cai, ZHANG Jie, ZHANG Liang, TIAN Ying, WU Guo-hua. Influence of heat treatment on microstructure and mechanical properties of as-cast Mg−8Li−3Al−2Zn−*x*Y alloy with duplex structure [J]. Materials Science and Engineering A, 2016, 669: 87−94.

[9] XU D K, WANG B J, LI C Q, ZU T T, HAN E H. Effect of icosahedral phase on the thermal stability and ageing response of a duplex structured Mg−Li alloy [J]. Materials & Design, 2015, 69: 124−129.

[10] ZHANG Cheng, WU Liang, ZHAO Zi-long, XIE Zhi-hui, HUANG Guang-sheng, LIU Lei, JIANG Bin, ATRENS A, PAN Fu-sheng. Effect of Li content on microstructure and mechanical property of Mg−*x*Li−3(Al−Si) alloys [J]. Transactions of Nonferrous Metals Society of China, 2019, 29(12): 2506−2513.

[11] ZHANG Jie, ZHANG Yang, WU Guo-hua, LIU Wen-cai, ZHANG Liang, DING Wen-jiang. Microstructure and mechanical properties of as-cast and extruded Mg−8Li−3Al−2Zn−0.5Nd alloy [J]. Materials Science and Engineering A, 2015, 621: 198−203.

[12] FEI Peng-fei, QU Zhi-kun, WU Rui-zhi. Microstructure and hardness of Mg−9Li−6Al−*x*La (*x*=0, 2, 5) alloys during solid solution treatment [J]. Materials Science and Engineering A, 2015, 625: 169−176.

[13] GUO Xu-ying, WU-Rui-zhi, ZHANG Jing-huai, LIU Bin, ZHANG Mi-lin. Influences of solid solution parameters on the microstructure and hardness of Mg−9Li−6Al and Mg−9Li−6Al−2Y [J]. Materials & Design, 2014, 53: 528−533.

[14] ZHAO Jiong, ZHANG Jie, LIU Wen-cai, WU Guo-hua, ZHANG Liang. Effect of Y content on microstructure and mechanical properties of as-cast Mg−8Li−3Al−2Zn alloy with duplex structure [J]. Materials Science and Engineering A, 2016, 650: 240−247.

[15] YANG Yan, PENG Xiao-dong, WEN Hai-ming, ZHENG Bao-long, ZHOU Yi-zhang, XIE Wei-dong, LAVERNIA E J. Influence of extrusion on the microstructure and mechanical behavior of Mg−9Li−3Al−*x*Sr alloys [J]. Metallurgical and Materials Transactions A, 2013, 44(2): 1101−1113.

[16] JIANG Bin, ZENG Ying, ZHANG Ming-xing, YIN Heng-mei, YANG Qing-shan, PAN Fu-sheng. Effects of Sn on microstructure of as-cast and as-extruded Mg−9Li alloys [J]. Transactions of Nonferrous Metals Society of China, 2013, 23(4): 904−908.

[17] KIM Y H, KIM J H, YU H S, CHOI J W, SON H T. Microstructure and mechanical properties of Mg−*x*Li−3Al−1Sn−0.4Mn alloys (*x*=5, 8 and 11, wt%) [J]. Journal of Alloys and Compounds, 2014, 583: 15−20.

[18] SON H T, KIM Y H, KIM D W, KIM J H, YU H S. Effects of Li addition on the microstructure and mechanical properties of Mg−3Zn−1Sn−0.4Mn based alloys [J]. Journal of Alloys and Compounds, 2013, 564: 130−137.

[19] FU Xue-song, YANG Yan, HU Jia-wei, SU Jun-fei, ZHANG Xue-ping, PENG Xiao-dong. Microstructure and mechanical properties of as-cast and extruded Mg−8Li−1Al− 0.5Sn alloy [J]. Materials Science and Engineering A, 2018, 709: 247−253.

[20] STJOHN D H, QIAN M, EASTON M A, CAO P, HILDEBRAND Z. Grain refinement of magnesium alloys [J]. Metallurgical and Materials Transactions A, 2005, 36(7): 1669−1679.

[21] JIANG Yan, CHEN Yu-an, FANG Dan, JIN Li. Effect of Li on microstructure, mechanical properties and fracture mechanism of as-cast Mg−5Sn alloy [J]. Materials Science and Engineering A, 2015, 641: 256−262.

[22] CHANG Li-li, SHI Chun-chang, CUI Hong-wei. Enhancement of mechanical properties of duplex Mg−9Li−3Al alloy by Sn and Y addition [J]. Transactions of Nonferrous Metals Society of China, 2018, 28(1): 30−35.

[23] LIU Gang, XIE Wen, HADADZADEH A, WEI Guo-bing, MA Zhen-duo, LIU Jun-wei, YANG Yan, XIE Wei-dong, PENG Xiao-dong, WELLS M. Hot deformation behavior and processing map of a superlight dual-phase Mg−Li alloy [J]. Journal of Alloys and Compounds, 2018, 766: 460−469.

[24] ZOU Yun, ZHANG Le-hao, WANG Hong-tao, TONG Xin, ZHANG Mi-lin, ZHANG Zhong-wu. Texture evolution and their effects on the mechanical properties of duplex Mg−Li alloy [J]. Journal of Alloys and Compounds, 2016, 669: 72−78.

[25] TONG L B, ZHENG M Y, CHENG L R, KAMADO S, ZHANG H J. Effect of extrusion ratio on microstructure, texture and mechanical properties of indirectly extruded Mg−Zn−Ca alloy [J]. Materials Science and Engineering A, 2013, 569: 48−53.

[26] XIAO Hong-chao, TANG Bei, LIU Chu-ming, GAO Yong-hao, YU Shi-lun, JIANG Shu-nong. Dynamic precipitation in a Mg−Gd−Y−Zr alloy during hot compression [J]. Materials Science and Engineering A, 2015, 645: 241−247.

[27] HUANG Hua, YUAN Guang-yin, CHEN Chun-lin, DING Wen-jiang, WANG Zhong-chang. Excellent mechanical properties of an ultrafine-grained quasicrystalline

strengthened magnesium alloy with multi-modal microstructure [J]. Materials Letters, 2013, 107: 181−184.
[28] ZHANG Yang, CHEN Xiao-yang, LU Ya-lin, LI Xiao-ping. Microstructure and mechanical properties of as-extruded Mg−Sn−Zn−Ca alloy with different extrusion ratios [J]. Transactions of Nonferrous Metals Society of China, 2018, 28(11): 2190−2198.
[29] JIA Qing-gong, ZHANG Wen-xin, SUN Yi, XU Chun-xiang, ZHANG Jin-shan, KUAN Jun. Microstructure and mechanical properties of as-cast and extruded biomedical Mg−Zn−Y−Zr−Ca alloy at different temperatures [J]. Transactions of Nonferrous Metals Society of China, 2019, 29(3): 515−525.
[30] ZHONG Li-ping, WANG Yong-jian. Microstructure evolution and optimum parameters analysis for hot working of new type Mg−8Sn−2Zn−0.5Cu alloy [J]. Transactions of Nonferrous Metals Society of China, 2019, 29(11): 2290−2299.

Sn 含量对铸态和挤压态 Mg−8Li−3Al−(1,2,3)Sn 合金显微组织和拉伸性能的影响

陈晓阳，张 扬，丛孟启，卢雅琳，李小平

江苏理工学院 江苏省先进材料设计与增材制造重点实验室，常州 213001

摘 要：采用 X 射线衍射、光学显微镜、扫描电镜和拉伸测试研究 Sn 含量对铸态和挤压态 Mg−8Li−3Al−(1,2,3)Sn (质量分数，%) 合金显微组织和拉伸性能的影响。研究发现，铸态 Mg−8Li−3Al−(1,2,3)Sn 合金由 α-Mg+β-Li 双相基体、$MgLiAl_2$ 相和 Li_2MgSn 相组成。Sn 含量的增加引起 α-Mg 枝晶细化和 Li_2MgSn 相含量增加。热挤压过程中，β-Li 相发生完全动态再结晶，而 α-Mg 相发生不完全动态再结晶。随 Sn 含量增加，α-Mg 相再结晶体积分数增加而再结晶晶粒平均尺寸减小。Sn 含量的增加能够提高铸态 Mg−8Li−3Al−(1,2,3)Sn 合金的强度，但对塑性不利。热挤压使 Mg−8Li−3Al−(1,2,3)Sn 合金的拉伸性能明显提高，Mg−8Li−3Al−2Sn 合金表现出最高的拉伸性能。

关键词：Mg−Li−Al−Sn 合金；铸态；再结晶；显微组织；拉伸性能

(Edited by Bing YANG)